LETTER

doi:10.1038/nature12050

A dust-obscured massive maximum-starburst galaxy at a redshift of 6.34

Dominik A. Riechers[1,2], C. M. Bradford[1,3], D. L. Clements[4], C. D. Dowell[1,3], I. Pérez-Fournon[5,6], R. J. Ivison[7,8], C. Bridge[1], A. Conley[9], Hai Fu[10], J. D. Vieira[1], J. Wardlow[10], J. Calanog[10], A. Cooray[1,10], P. Hurley[11], R. Neri[12], J. Kamenetzky[13], J. E. Aguirre[14], B. Altieri[15], V. Arumugam[8], D. J. Benford[16], M. Béthermin[17,18], J. Bock[1,3], D. Burgarella[19], A. Cabrera-Lavers[5,6,20], S. C. Chapman[21], P. Cox[12], J. S. Dunlop[8], L. Earle[9], D. Farrah[22], P. Ferrero[5,6], A. Franceschini[23], R. Gavazzi[24], J. Glenn[9,13], E. A. Gonzalez Solares[21], M. A. Gurwell[25], M. Halpern[26], E. Hatziminaoglou[27], A. Hyde[4], E. Ibar[7], A. Kovács[1,28], M. Krips[12], R. E. Lupu[14], P. R. Maloney[9], P. Martinez-Navajas[5,6], H. Matsuhara[29], E. J. Murphy[1,30], B. J. Naylor[3], H. T. Nguyen[1,3], S. J. Oliver[11], A. Omont[24], M. J. Page[31], G. Petitpas[25], N. Rangwala[13], I. G. Roseboom[8,11], D. Scott[26], A. J. Smith[11], J. G. Staguhn[16,32], A. Streblyanska[5,6], A. P. Thomson[8], I. Valtchanov[15], M. Viero[1], L. Wang[11], M. Zemcov[1,3] & J. Zmuidzinas[1,3]

Massive present-day early-type (elliptical and lenticular) galaxies probably gained the bulk of their stellar mass and heavy elements through intense, dust-enshrouded starbursts—that is, increased rates of star formation—in the most massive dark-matter haloes at early epochs. However, it remains unknown how soon after the Big Bang massive starburst progenitors exist. The measured redshift (z) distribution of dusty, massive starbursts has long been suspected to be biased low in z owing to selection effects[1], as confirmed by recent findings of systems with redshifts as high as ~5 (refs 2–4). Here we report the identification of a massive starburst galaxy at $z = 6.34$ through a submillimetre colour-selection technique. We unambiguously determined the redshift from a suite of molecular and atomic fine-structure cooling lines. These measurements reveal a hundred billion solar masses of highly excited, chemically evolved interstellar medium in this galaxy, which constitutes at least 40 per cent of the baryonic mass. A 'maximum starburst' converts the gas into stars at a rate more than 2,000 times that of the Milky Way, a rate among the highest observed at any epoch. Despite the overall downturn in cosmic star formation towards the highest redshifts[5], it seems that environments mature enough to form the most massive, intense starbursts existed at least as early as 880 million years after the Big Bang.

We have searched 21 deg^2 of the Herschel/SPIRE data of the HerMES blank field survey[6] at wavelengths 250–500 μm for 'ultra-red' sources with flux densities $S_{250\mu m} < S_{350\mu m} < S_{500\mu m}$ and $S_{500\mu m}/S_{350\mu m} > 1.3$, that is, galaxies that are significantly redder (and thus, potentially at higher redshift) than massive starbursts discovered thus far. This selection yields five candidate ultra-red sources down to a flux limit of 30 mJy at 500 μm (>5σ and above the confusion noise; see Supplementary Information section 1 for additional details), corresponding to a source density of ≤0.24 deg^{-2}. For comparison, models of number counts in the Herschel/SPIRE bands suggest a space density of massive starburst galaxies at $z > 6$ with $S_{500\mu m} > 30$ mJy of 0.014 deg^{-2} (ref. 7).

To understand the nature of galaxies selected by this technique, we have obtained full frequency scans of the 3-mm and 1-mm bands towards HFLS 3 (also known as 1HERMES S350 J170647.8+584623; $S_{500\mu m}/S_{350\mu m} = 1.45$), the brightest candidate discovered in our study. These observations, augmented by selected follow-up over a broader wavelength range, unambiguously determine the galaxy redshift to be $z = 6.3369 \pm 0.0009$ based on a suite of 7 CO lines, 7 H_2O lines, and OH, OH^+, H_2O^+, NH_3, [C I] and [C II] lines detected in emission and absorption (Fig. 1). At this redshift, the Universe was just 880 million years old (or one-sixteenth of its present age), and 1″ on the sky corresponds to a physical scale of 5.6 kpc. Further observations from optical to radio wavelengths reveal strong continuum emission over virtually the entire wavelength range between 2.2 μm and 20 cm, with no detected emission shortward of 1 μm (see Supplementary Information section 2 and Supplementary Figs 1–11 for additional details).

HFLS 3 hosts an intense starburst. The 870-μm flux of HFLS 3 is >3.5 times higher than those of the brightest high-redshift starbursts in a 0.25-deg^2 region containing the Hubble Ultra Deep Field (HUDF)[8]. From the continuum spectral energy distribution (Fig. 2), we find that the far-infrared (FIR) luminosity L_{FIR} and inferred star formation rate (SFR) of 2,900 M_{sun} yr^{-1} of HFLS 3 (where M_{sun} is the solar mass) are 15–20 times those of the prototypical local ultra-luminous starburst Arp 220, and >2,000 times those of the Milky Way (Table 1 and Supplementary Information section 3). The SFR of HFLS 3 alone corresponds to ~4.5 times the ultraviolet-based SFR of all $z = 5.5$–6.5 star-forming galaxies in the HUDF combined[9], but the rarity and dust obscuration of ultra-red sources like HFLS 3 implies that they do not dominate the ultraviolet photon density needed to reionize the Universe[10].

[1]California Institute of Technology, 1200 East California Boulevard, MC 249-17, Pasadena, California 91125, USA. [2]Cornell University, 220 Space Sciences Building, Ithaca, New York 14853, USA. [3]Jet Propulsion Laboratory, 4800 Oak Grove Drive, Pasadena, California 91109, USA. [4]Astrophysics Group, Imperial College London, Blackett Laboratory, Prince Consort Road, London SW7 2AZ, UK. [5]Instituto de Astrofisica de Canarias, E-38200 La Laguna, Tenerife, Spain. [6]Departamento de Astrofisica, Universidad de La Laguna, E-38205 La Laguna, Tenerife, Spain. [7]UK Astronomy Technology Centre, Royal Observatory, Blackford Hill, Edinburgh EH9 3HJ, UK. [8]Institute for Astronomy, University of Edinburgh, Royal Observatory, Blackford Hill, Edinburgh EH9 3HJ, UK. [9]Center for Astrophysics and Space Astronomy 389-UCB, University of Colorado, Boulder, Colorado 80309, USA. [10]Department of Physics and Astronomy, University of California, Irvine, California 92697, USA. [11]Astronomy Centre, Department of Physics and Astronomy, University of Sussex, Brighton BN1 9QH, UK. [12]Institut de RadioAstronomie Millimetrique, 300 Rue de la Piscine, Domaine Universitaire, F-38406 Saint Martin d'Heres, France. [13]Department of Astrophysical and Planetary Sciences, CASA 389-UCB, University of Colorado, Boulder, Colorado 80309, USA. [14]Department of Physics and Astronomy, University of Pennsylvania, Philadelphia, Pennsylvania 19104, USA. [15]Herschel Science Centre, European Space Astronomy Centre, Villanueva de la Cañada, 28691 Madrid, Spain. [16]Observational Cosmology Laboratory, Code 665, NASA Goddard Space Flight Center, Greenbelt, Maryland 20771, USA. [17]Laboratoire AIM-Paris-Saclay, CEA/DSM/Irfu – CNRS – Université Paris Diderot, CEA Saclay, Point courrier 131, F-91191 Gif-sur-Yvette, France. [18]Institut d'Astrophysique Spatiale (IAS), Bâtiment 121, Universite Paris-Sud 11 and CNRS, UMR 8617, F-91405 Orsay, France. [19]Aix-Marseille Université, CNRS, Laboratoire d'Astrophysique de Marseille, UMR7326, F-13388 Marseille, France. [20]Grantecan S.A., Centro de Astrofísica de La Palma, Cuesta de San Jose, E-38712 Brena Baja, La Palma, Spain. [21]Institute of Astronomy, University of Cambridge, Madingley Road, Cambridge CB3 0HA, UK. [22]Department of Physics, Virginia Tech, Blacksburg, Virginia 24061, USA. [23]Dipartimento di Fisica e Astronomia, Università di Padova, vicolo Osservatorio 3, I-35122 Padova, Italy. [24]Institut d'Astrophysique de Paris, UMR 7095, CNRS, UPMC Univ. Paris 06, 98bis Boulevard Arago, F-75014 Paris, France. [25]Harvard-Smithsonian Center for Astrophysics, 60 Garden Street, Cambridge, Massachusetts 02138, USA. [26]Department of Physics and Astronomy, University of British Columbia, 6224 Agricultural Road, Vancouver, British Columbia V6T 1Z1, Canada. [27]ESO, Karl-Schwarzschild-Strasse 2, D-85748 Garching bei München, Germany. [28]Institute for Astrophysics, University of Minnesota, 116 Church Street Southeast, Minneapolis, Minnesota 55455, USA. [29]Institute for Space and Astronautical Science, Japan Aerospace and Exploration Agency, Sagamihara, Kanagawa 229-8510, Japan. [30]Infrared Processing and Analysis Center, MS 100-22, California Institute of Technology, Pasadena, California 91125, USA. [31]Mullard Space Science Laboratory, University College London, Holmbury St Mary, Dorking RH5 6NT, UK. [32]Department of Physics and Astronomy, Johns Hopkins University, Baltimore, Maryland 21218, USA.

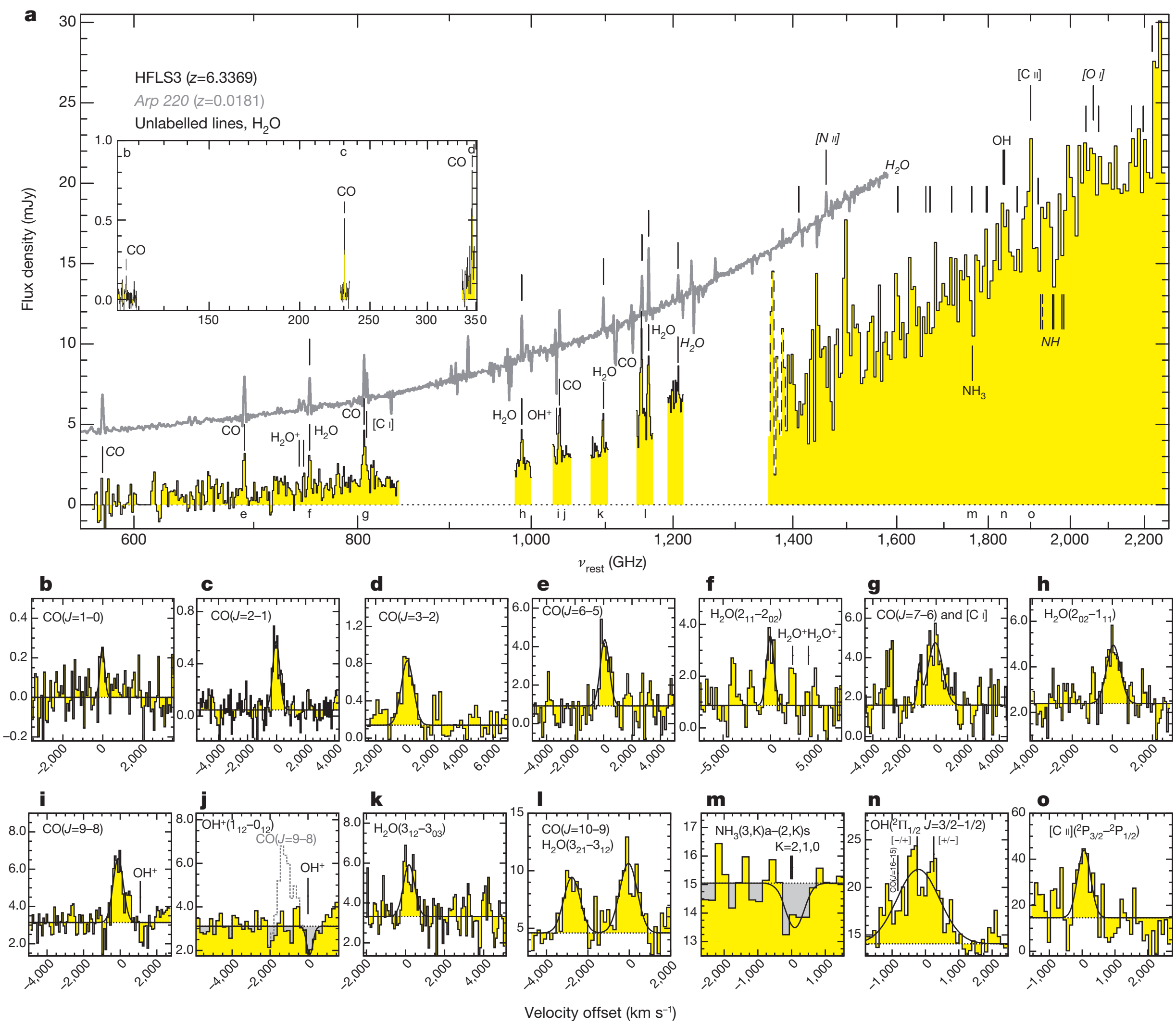

Figure 1 | Redshift identification through molecular and atomic spectroscopy of HFLS 3. **a**, Black trace, wide-band spectroscopy in the observed-frame 19–0.95-mm (histogram; rest-frame 2,600–130 μm) wavelength range with CARMA (3 mm; 'blind' frequency scan of the full band), the PdBI (2 mm), the JVLA (19–6 mm) and CSO/Z-spec (1 mm; instantaneous coverage). (CARMA, Combined Array for Research in Millimeter-wave Astronomy; PdBI, Plateau de Bure Interferometer; JVLA, Jansky Very Large Array; and CSO, Caltech Submillimeter Observatory.) This uniquely determines the redshift of HFLS 3 to be $z = 6.3369$ based on the detection of a series of H_2O, CO, OH, OH^+, NH_3, [C I] and [C II] emission and absorption lines. **b**–**o**, Detailed profiles of detected lines (histograms; rest frequencies are indicated by corresponding letters in **a**). 1-mm lines (**m**–**o**) are deeper, interferometric confirmation observations for NH_3, OH (both PdBI) and [C II] (CARMA) not shown in **a**. The line profiles are typically asymmetric relative to single Gaussian fits, indicating the presence of two principal velocity components at redshifts of 6.3335 and 6.3427. The implied CO, [C I] and [C II] line luminosities are respectively $(5.08 \pm 0.45) \times 10^6\,L_{sun}$, $(3.0 \pm 1.9) \times 10^8\,L_{sun}$ and $(1.55 \pm 0.32) \times 10^{10}\,L_{sun}$. Strong rest-frame submillimetre to FIR continuum emission is detected over virtually the entire wavelength range. For comparison, the Herschel/SPIRE spectrum of the nearby ultra-luminous infrared galaxy Arp 220[20] is overplotted in grey (**a**). Lines labelled in italic are tentative detections or upper limits (see Supplementary Table 2). Most of the bright spectral features detected in Arp 220[20,21] are also detected in HFLS 3 (in spectral regions not blocked by the terrestrial atmosphere). See Supplementary Information sections 2–4 for more details.

HFLS 3 is a massive, gas-rich galaxy. From the spectral energy distribution and the intensity of the CO and [C II] emission, we find a dust mass of $M_d = 1.3 \times 10^9\,M_{sun}$ and total molecular and atomic gas masses of respectively $M_{gas} = 1.0 \times 10^{11}\,M_{sun}$ and $M_{HI} = 2.0 \times 10^{10}\,M_{sun}$. These masses are 15–20 times those of Arp 220, and correspond to a gas-to-dust ratio of ~80 and a gas depletion timescale of $M_{gas}/SFR \approx 36$ Myr. These values are comparable to lower-redshift submillimetre-selected starbursts[11,12]. From the [C I] luminosity, we find an atomic carbon mass of $4.5 \times 10^7\,M_{sun}$. At the current SFR of HFLS 3, this level of carbon enrichment could have been achieved through supernovae on a timescale of $\sim 10^7$ yr (ref. 13). The profiles of the molecular and atomic emission lines typically show two velocity components (Fig. 1 and Supplementary Figs 5 and 7). The gas is distributed over a region of 1.7 kpc radius with a high velocity gradient and dispersion (Fig. 3). This suggests a dispersion-dominated galaxy with a dynamical mass of $M_{dyn} = 2.7 \times 10^{11}\,M_{sun}$. The gas mass fraction in galaxies is a measure of the relative depletion and replenishment of molecular gas, and is expected to be a function of halo mass and redshift from simulations[14]. In HFLS 3, we find a high gas mass fraction of $f_{gas} = M_{gas}/M_{dyn} \approx 40\%$, comparable to what is found in submillimetre-selected starbursts and massive star-forming galaxies at $z \approx 2$ (refs 15, 16), but ~3 times higher than in nearby ultra-luminous infrared galaxies (ULIRGs) like Arp 220, and >30 times higher than in the Milky Way. From population synthesis modelling, we find a stellar mass of $M_* = 3.7 \times 10^{10}\,M_{sun}$, comparable to that of Arp 220 and about half that of the Milky Way. This suggests that at most ~40% of M_{dyn} within the radius of the gas reservoir is due to dark matter. With up to $\sim 10^{11}\,M_{sun}$ of dark matter within 3.4 kpc, HFLS 3 is likely to reside in a dark-matter halo massive enough to grow a present-day galaxy cluster[17]. The efficiency of star formation is given by $\varepsilon = t_{dyn} \times SFR/M_{gas}$, where $t_{dyn} = (r^3/(2GM))^{1/2}$ is the dynamical (or free-fall) time, r is the source radius,

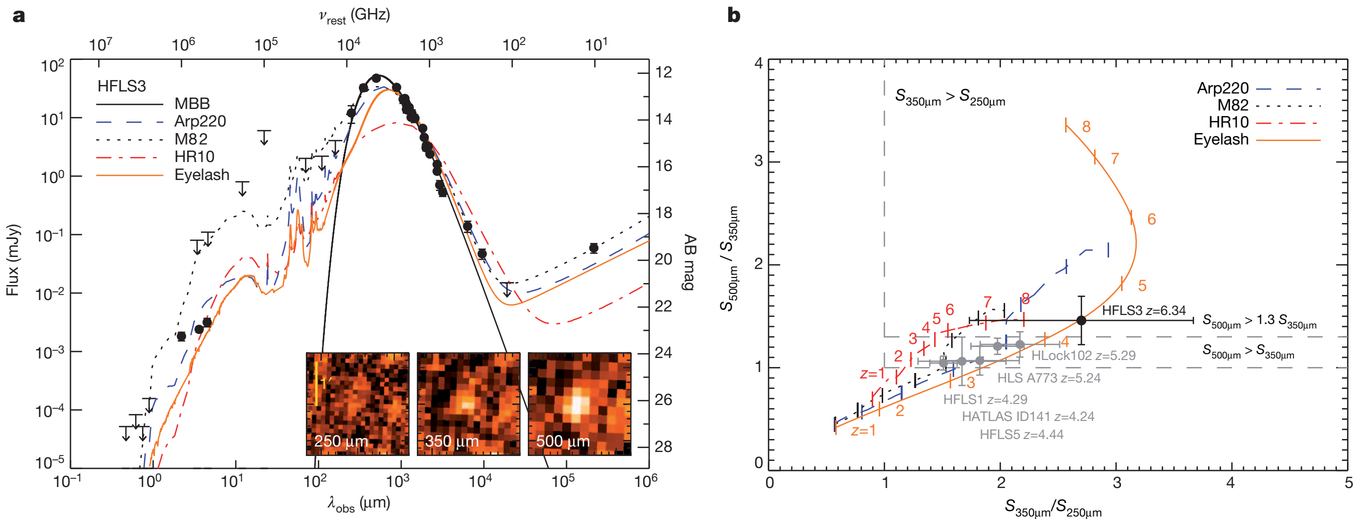

Figure 2 | Spectral energy distribution and Herschel/SPIRE colours of HFLS 3. **a**, HFLS 3 was identified as a very high redshift candidate, as it appears red between the Herschel/SPIRE 250-, 350- and 500-µm bands (inset). The spectral energy distribution of the source (data points; λ_{obs}, observed-frame wavelength; ν_{rest}, rest-frame frequency; AB mag, magnitudes in the AB system; error bars are 1σ r.m.s. uncertainties in both panels) is fitted with a modified black body (MBB; solid line) and spectral templates for the starburst galaxies Arp 220, M 82, HR 10 and the Eyelash (broken lines, see key). The implied FIR luminosity is $2.86^{+0.32}_{-0.31} \times 10^{13}\ L_{sun}$. The dust in HFLS 3 is not optically thick at wavelengths longward of rest-frame 162.7 µm (95.4% confidence; Supplementary Fig. 12). This is in contrast to Arp 220, in which the dust becomes optically thick (that is, $\tau_d = 1$) shortward of 234 ± 3 µm (ref. 20). Other high-redshift massive starburst galaxies (including the Eyelash) typically become optically thick around ~200 µm. This suggests that none of the detected molecular/fine-structure emission lines in HFLS 3 require correction for extinction. The radio continuum luminosity of HFLS 3 is consistent with the radio–FIR correlation for nearby star-forming galaxies. **b**, Flux density ratios (350 µm/250 µm and 500 µm/350 µm) of HFLS 3. The coloured lines are the same templates as in **a**, but redshifted between $1 < z < 8$ (number labels indicate redshifts). Dashed grey lines indicate the dividing lines for red ($S_{250µm} < S_{350µm} < S_{500µm}$) and ultra-red ($S_{250µm} < S_{350µm}$ and $1.3 \times S_{350µm} < S_{500µm}$) sources. Grey symbols show the positions of five spectroscopically confirmed red sources at $4 < z < 5.5$ (including three new sources from our study), which all fall outside the ultra-red cut-off. This shows that ultra-red sources will lie at $z > 6$ for typical shapes of the spectral energy distribution (except those with low dust temperatures), whereas red sources typically are at $z < 5.5$. See Supplementary Information sections 1 and 3 for more details.

M is the mass within radius r and G is the gravitational constant. For $r = 1.7$ kpc and $M = M_{gas}$, this suggests $\varepsilon = 0.06$, which is a few times higher than found in nearby starbursts and in giant molecular cloud cores in the Galaxy[18].

The properties of atomic and molecular gas in HFLS 3 are fully consistent with a highly enriched, highly excited interstellar medium,

Table 1 | Observed and derived quantities for HFLS 3, Arp 220 and the Milky Way

	HFLS 3	Arp 220*	Milky Way*
z	6.3369	0.0181	
M_{gas} (M_{sun})†	$(1.04 \pm 0.09) \times 10^{11}$	5.2×10^9	2.5×10^9
M_{dust} (M_{sun})‡	$1.31^{+0.32}_{-0.30} \times 109$	$\sim 1 \times 10^8$	$\sim 6 \times 10^7$
M_* (M_{sun})§	$\sim 3.7 \times 10^{10}$	$\sim (3–5) \times 10^{10}$	$\sim 6.4 \times 10^{10}$
M_{dyn} (M_{sun}) ∥	2.7×10^{11}	3.45×10^{10}	2×10^{11} (<20 kpc)
f_{gas} (%)¶	40	15	1.2
L_{FIR} (L_{sun})#	$2.86^{+0.32}_{-0.31} \times 10^{13}$	1.8×10^{12}	1.1×10^{10}
SFR ($M_{sun}\ yr^{-1}$)☆	2,900	~180	1.3
T_{dust} (K)**	$55.9^{+9.3}_{-12.0}$	66	~19

For details see Supplementary Information section 3.
* Literature values for Arp 220 and the Milky Way are adopted from refs 20 and 27–30. The total molecular gas mass of the Milky Way is uncertain by at least a factor of 2. Quoted dust masses and stellar masses are typically uncertain by factors of 2–3 owing to systematics. The dynamical mass for the Milky Way is quoted within the inner 20 kpc to be comparable to the other systems, not probing the outer regions dominated by dark matter. The dust temperature in the Milky Way varies by at least ±5 K around the quoted value, which is used as a representative value. Both Arp 220 and the Milky Way are known to contain small fractions of significantly warmer dust. All errors are 1σ r.m.s. uncertainties.
† Molecular gas mass, derived assuming $\alpha_{CO} = M_{gas}/L'_{CO} = 1\ M_{sun}$ (K km s^{-1} pc^2)$^{-1}$ (see Supplementary Information section 3.3).
‡ Dust mass, derived from spectral energy distribution fitting (see Supplementary Information section 3.1).
§ Stellar mass, derived from population synthesis fitting (see Supplementary Information section 3.4).
∥ Dynamical mass (see Supplementary Information section 3.5).
¶ Gas mass fraction, derived assuming $f_{gas} = M_{gas}/M_{dyn}$ (see Supplementary Information section 3.6).
# FIR luminosity as determined over the range of 42.5–122.5 µm from spectral energy distribution fitting (see Supplementary Information section 3.1).
☆ SFR, derived assuming SFR (in $M_{sun}\ yr^{-1}$) = $1.0 \times 10^{-10}\ L_{FIR}$ (in L_{sun}) (see Supplementary Information section 3.2).
** Dust temperature, derived from spectral energy distribution fitting (see Supplementary Information section 3.1).

as typically found in the nuclei of warm, intense starbursts, but distributed over a large, ~3.5-kpc-diameter, region. The observed CO and [C II] luminosities suggest that dust is the primary coolant of the gas if both are thermally coupled. The $L_{[CII]}/L_{FIR}$ ratio of $\sim 5 \times 10^{-4}$ is typical for high radiation environments in extreme starbursts and active galactic nucleus (AGN) host galaxies[19]. The $L_{[CII]}/L_{CO(1-0)}$ ratio of ~3,000 suggests that the bulk of the line emission is associated with the photon-dominated regions of a massive starburst. At the L_{FIR} of HFLS 3, this suggests an infrared radiation field strength and gas density comparable to nearby ULIRGs without luminous AGN (figures 4 and 5 of ref. 19).

From the spectral energy distribution of HFLS 3, we derive a dust temperature of $T_{dust} = 56^{+9}_{-12}$K, ~10 K less than in Arp 220, but ~3 times that of the Milky Way. CO radiative transfer models assuming collisional excitation suggest a gas kinetic temperature of $T_{kin} = 144^{+59}_{-30}$K and a gas density of $\log_{10}(n(H_2)) = 3.80^{+0.28}_{-0.17}$ cm^{-3} (Supplementary Information section 4 and Supplementary Figs 13 and 14). These models suggest similar gas densities as in nearby ULIRGs, and prefer $T_{kin} \gg T_{dust}$, which may imply that the gas and dust are not in thermal equilibrium, and that the excitation of the molecular lines may be partially supported by the underlying infrared radiation field. This is consistent with the finding that we detect H_2O and OH lines with upper level energies of $E/k_B > 300–450$ K and critical densities of $>10^{8.5}$ cm^{-3} at line intensities exceeding those of the CO lines. The intensities and ratios of the detected H_2O lines cannot be reproduced by radiative transfer models assuming collisional excitation, but are consistent with being radiatively pumped by FIR photons, at levels comparable to those observed in Arp 220 (Supplementary Figs 15 and 16)[20,21]. The CO and H_2O excitation is inconsistent with what is observed in quasar host galaxies like Mrk 231 and APM 08279+5255 at $z = 3.9$, which lends support to the conclusion that the gas is excited by a mix of collisions and infrared photons associated with a massive, intense starburst, rather than hard radiation associated with a luminous AGN[22]. The physical

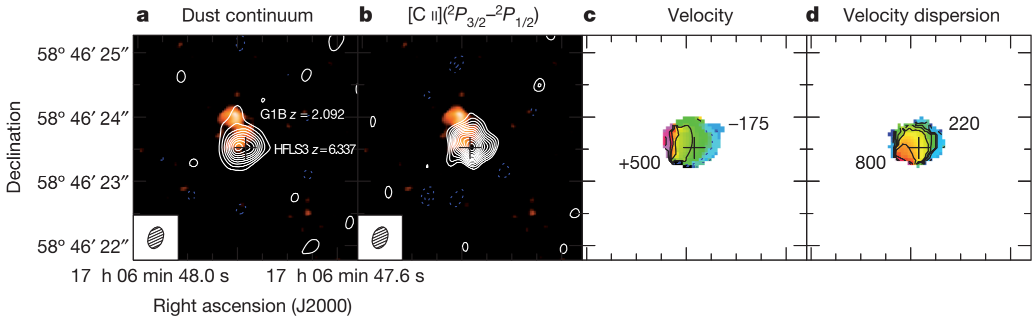

Figure 3 | Gas dynamics, dust obscuration, and distribution of gas and star formation in HFLS 3. **a**, **b**, High-resolution (FWHM 0.35″ × 0.23″) maps of the 158-μm continuum (**a**) and [C II] line emission (**b**) obtained at 1.16 mm with the PdBI in A-configuration, overlaid on a Keck/NIRC2 2.2-μm adaptive optics image (rest-frame ultraviolet/optical light). The r.m.s. uncertainty in the continuum (**a**) and line (**b**) maps is 180 and 400 μJy per beam, and contours are shown in steps of 3σ and 1σ, starting at 5σ and 3σ, respectively. A $z = 2.092$ galaxy (labelled G1B) identified through Keck/LRIS spectroscopy is detected ~0.65″ north of HFLS 3, but is not massive enough to cause significant gravitational lensing at the position of HFLS 3. Faint infrared emission is detected towards a region with lower dust obscuration in the northeastern part of HFLS 3 (not detected at <1 μm). The Gaussian diameters of the resolved [C II] and continuum emission are 3.4 kpc × 2.9 kpc and 2.6 kpc × 2.4 kpc, suggesting gas and SFR surface densities of $\Sigma_{gas} = 1.4 \times 10^4 M_{sun} pc^{-2}$ and $\Sigma_{SFR} = 600 M_{sun} yr^{-1} kpc^{-2}$ ($\sim 0.6 \times 10^{13} L_{sun} kpc^{-2}$). The high Σ_{SFR} is consistent with a maximum starburst at near-Eddington-limited intensity. Given the moderate optical depth of $\tau_d < \sim 1$ at 158 μm, this estimate is somewhat conservative. **c**, **d**, Peak velocity (**c**) and FWHM velocity dispersion (**d**) maps of the [C II] emission are obtained by Gaussian fitting to the line emission in each spatial point of the map. Velocity contours are shown in steps of 100 km s^{-1}. High-resolution CO $J = 7$–6 and 10–9 and H_2O 3_{21}–3_{12} observations show consistent velocity profiles and velocity structure (Supplementary Figs 5–7). The large velocity dispersion suggests that the gas dynamics in this system are dispersion-dominated. See Supplementary Information sections 3 and 5 for more details.

conditions in the ISM of HFLS 3 thus are comparable to those in the nuclei of the most extreme nearby starbursts, consistent with the finding that it follows the radio–FIR correlation for star-forming galaxies.

HFLS 3 is rapidly assembling its stellar bulge through star formation at surface densities close to the theoretically predicted limit for 'maximum starbursts'[23]. At a rest-frame wavelength of 158 μm, the FIR emission is distributed over a relatively compact area with 2.6 kpc × 2.4 kpc physical diameter along its major and minor axes respectively (Fig. 3; as determined by elliptical Gaussian fitting). This suggests an extreme SFR surface density of $\Sigma_{SFR} \approx 600 M_{sun} yr^{-1} kpc^{-2}$ over a 1.3-kpc-radius region, and is consistent with near-Eddington-limited star formation if the starburst disk is supported by radiation pressure[24]. This suggests the presence of a kiloparsec-scale hyper-starburst similar to that found in the $z = 6.42$ quasar J1148+5251 (ref. 25). Such high Σ_{SFR} are also observed in the nuclei of local ULIRGs such as Arp 220, albeit on scales two orders of magnitude smaller. A starburst at such high Σ_{SFR} may produce strong winds. Indeed, the relative strength and broad, asymmetric profile of the OH $^2\Pi_{1/2}$(3/2–1/2) doublet detected in HFLS 3 may indicate a molecular outflow, reminiscent of the OH outflow in Arp 220[21].

The identification of HFLS 3 alone is still consistent with the model-predicted space density of massive starburst galaxies at $z > 6$ with $S_{500\mu m} > 30$ mJy of 0.014 deg^{-2} (ref. 7). This corresponds to only 10^{-3}–10^{-4} times the space density of Lyman-break galaxies at the same redshift, but is comparable to the space density of the most luminous quasars hosting supermassive black holes (that is, a different population of massive galaxies) at such early cosmic times[26]. The host galaxies around these very distant supermassive black holes are commonly FIR-luminous, but less intensely star-forming, with typically a few times lower L_{FIR} than ultra-red sources[25]. This highlights the difference between selecting massive $z > 6$ galaxies at the peak of their star formation activity through L_{FIR}, and at the peak of their black-hole activity through luminous AGN. The substantial population of ultra-red sources discovered with Herschel will be an ideal probe of early galaxy evolution and heavy element enrichment within the first billion years of cosmic time. These galaxies are unlikely to dominate the star formation history of the Universe at $z > 6$ (ref. 5), but they trace the highest peaks in SFR at early epochs. A detailed study of this galaxy population will reveal the mass and redshift distribution, number density and likely environments of such objects, which if confirmed in larger numbers may present a stern challenge to current models of early cosmic structure formation.

Received 4 October 2012; accepted 27 February 2013.

1. Chapman, S. C. *et al.* A median redshift of 2.4 for galaxies bright at submillimetre wavelengths. *Nature* **422,** 695–698 (2003).
2. Capak, P. *et al.* A massive protocluster of galaxies at a redshift of $z \approx 5.3$. *Nature* **470,** 233–235 (2011).
3. Walter, F. *et al.* The intense starburst HDF 850.1 in a galaxy overdensity at $z \approx 5.2$ in the Hubble Deep Field. *Nature* **486,** 233–236 (2012).
4. Vieira, J. D. *et al.* Dusty starburst galaxies in the early Universe as revealed by gravitational lensing. *Nature* **495,** 344–347 (2013).
5. Bouwens, R. *et al.* A candidate redshift $z \approx 10$ galaxy and rapid changes in that population at an age of 500 Myr. *Nature* **469,** 504–507 (2011).
6. Oliver, S. *et al.* The Herschel Multi-tiered Extragalactic Survey: HerMES. *Mon. Not. R. Astron. Soc.* **424,** 1614–1635 (2012).
7. Béthermin, M. *et al.* A unified empirical model for infrared galaxy counts based on the observed physical evolution of distant galaxies. *Astrophys. J.* **757,** L23 (2012).
8. Karim, A. *et al.* An ALMA survey of submillimetre galaxies in the Extended Chandra Deep Field South: high resolution 870μm source counts. *Mon. Not. R. Astron. Soc.* (in the press); preprint at http://arxiv.org/abs/1210.0249 (2012).
9. Bouwens, R. J. *et al.* Galaxies at z ~ 6: the UV luminosity function and luminosity density from 506 HUDF, HUDF parallel ACS field, and GOODS i-dropouts. *Astrophys. J.* **653,** 53–85 (2006).
10. Robertson, B. *et al.* Early star-forming galaxies and the reionization of the Universe. *Nature* **468,** 49–55 (2010).
11. Michałowski, M. J. *et al.* Rapid dust production in submillimeter galaxies at z > 4? *Astrophys. J.* **712,** 942–950 (2010).
12. Riechers, D. A. *et al.* Extended cold molecular gas reservoirs in z ~ 3.4 submillimeter galaxies. *Astrophys. J.* **739,** L31 (2011).
13. Walter, F. *et al.* Molecular gas in the host galaxy of a quasar at redshift z = 6.42. *Nature* **424,** 406–408 (2003).
14. Lagos, C. & Del P. *et al.* On the impact of empirical and theoretical star formation laws on galaxy formation. *Mon. Not. R. Astron. Soc.* **416,** 1566–1584 (2011).
15. Tacconi, L. J. *et al.* Submillimeter galaxies at z ~ 2: evidence for major mergers and constraints on lifetimes, IMF, and CO-H_2 conversion factor. *Astrophys. J.* **680,** 246–262 (2008).
16. Tacconi, L. J. *et al.* High molecular gas fractions in normal massive star-forming galaxies in the young Universe. *Nature* **463,** 781–784 (2010).
17. Overzier, R. *et al.* ΛCDM predictions for galaxy protoclusters – I. The relation between galaxies, protoclusters and quasars at z ~ 6. *Mon. Not. R. Astron. Soc.* **394,** 577–594 (2009).
18. Krumholz, M. R. *et al.* A universal, local star formation law in galactic clouds, nearby galaxies, high-redshift disks, and starbursts. *Astrophys. J.* **745,** 69 (2012).
19. Stacey, G. J. *et al.* A 158 μm [C II] line survey of galaxies at z ~ 1–2: an indicator of star formation in the early universe. *Astrophys. J.* **724,** 957–974 (2010).
20. Rangwala, N. *et al.* Observations of Arp 220 using Herschel-SPIRE: an unprecedented view of the molecular gas in an extreme star formation environment. *Astrophys. J.* **743,** 94 (2011).

21. Gonzalez-Alfonso, E. *et al.* Herschel/PACS spectroscopy of NGC 4418 and Arp 220: H_2O, $H_2{}^{18}O$, OH, ^{18}OH, O I, HCN and NH_3. *Astron. Astrophys.* **541,** A4 (2012).
22. van der Werf, P. *et al.* Water vapor emission reveals a highly obscured, star-forming nuclear region in the QSO host galaxy APM 08279+5255 at $z = 3.9$. *Astrophys. J.* **741,** L38 (2011).
23. Elmegreen, B. G. Galactic bulge formation as a maximum intensity starburst. *Astrophys. J.* **517,** 103–107 (1999).
24. Thompson, T. *et al.* Radiation pressure-supported starburst disks and active galactic nucleus fueling. *Astrophys. J.* **630,** 167–185 (2005).
25. Walter, F. *et al.* A kiloparsec-scale hyper-starburst in a quasar host less than 1 gigayear after the Big Bang. *Nature* **457,** 699–701 (2009).
26. Jiang, L. *et al.* A survey of $z \sim 6$ quasars in the Sloan Digital Sky Survey deep stripe. II. Discovery of six quasars at $z_{AB}>21$. *Astron. J.* **138,** 305–311 (2009).
27. Downes, D. & Solomon, P. M. Rotating nuclear rings and extreme starbursts in ultraluminous galaxies. *Astrophys. J.* **507,** 615–654 (1998).
28. Sodroski, T. J. *et al.* Large-scale characteristics of interstellar dust from COBE DIRBE observations. *Astrophys. J.* **428,** 638–646 (1994).
29. Murray, N. & Rahman, M. Star formation in massive clusters via the Wilkinson Microwave Anisotropy Probe and the Spitzer Glimpse survey. *Astrophys. J.* **709,** 424–435 (2010).
30. McMillan, P. J. Mass models of the Milky Way. *Mon. Not. R. Astron. Soc.* **414,** 2446–2457 (2011).

Supplementary Information is available in the online version of the paper.

Acknowledgements Herschel is an ESA space observatory with science instruments provided by European-led Principal Investigator consortia and with important participation from NASA. This research has made use of data from the HerMES project. HerMES is a Herschel Key Programme using guaranteed time from the SPIRE instrument team, ESAC scientists and a mission scientist. See Supplementary Information for further acknowledgements.

Author Contributions D.A.R. had the overall lead of the project. C.M.B., D.L.C., I.P.-F., R.J.I., C.B., H.F., J.D.V. and R.N. contributed significantly to the taking and analysis of the follow-up data with different instruments by leading several telescope proposals and analysis efforts. C.D.D. led the selection of the parent sample. A. Conley, J.W., J.C., A. Cooray, P.H. and J.K. contributed significantly to the data analysis and to fitting and modelling the results. All other authors contributed to the proposals, source selection, data analysis and interpretation, in particular through work on the primary Herschel SPIRE data in which the source was discovered through the HerMES consortium (led by J.B. and S.J.O.). All authors have reviewed, discussed, and commented on the manuscript.

Author Information Reprints and permissions information is available at www.nature.com/reprints. The authors declare no competing financial interests. Readers are welcome to comment on the online version of the paper. Correspondence and requests for materials should be addressed to D.A.R. (dr@astro.cornell.edu).